

# Towards a measurement of the emittance of muons produced by positron annihilation at threshold energy

---

N. Amapane,<sup>a,b</sup> M. Antonelli,<sup>c</sup> F. Anulli,<sup>d</sup> G. Ballerini,<sup>e,f</sup> L. Bandiera,<sup>g</sup> N. Bartosik,<sup>b</sup> M. Bauce,<sup>d</sup> A. Bertolin,<sup>h</sup> C. Biino,<sup>b</sup> O. R. Blanco-Garcia,<sup>c</sup> M. Boscolo,<sup>c</sup> C. Brizzolari,<sup>e,f</sup> A. Cappati,<sup>a,b</sup> M. Casarsa,<sup>i</sup> G. Cavoto,<sup>l,d</sup> F. Collamati,<sup>d</sup> G. Cotto,<sup>a,b</sup> C. Curatolo,<sup>h</sup> R. Di Nardo,<sup>m</sup> F. Gonella,<sup>h</sup> S. Hoh,<sup>n,h</sup> M. Iafrafi,<sup>c</sup> F. Iacoangeli,<sup>d</sup> B. Kiani,<sup>b</sup> D. Lucchesi,<sup>n,h</sup> V. Mascagna,<sup>e,f</sup> A. Paccagnella,<sup>n,h</sup> N. Pastrone,<sup>b</sup> J. Pazzini,<sup>n,h</sup> M. Pelliccioni,<sup>b</sup> B. Ponzio,<sup>c</sup> M. Prest,<sup>e,f</sup> M. Ricci,<sup>c</sup> R. Rossin,<sup>n,h</sup> M. Rotondo,<sup>c</sup> O. Sans Planell,<sup>a,b</sup> L. Sestini,<sup>h</sup> M. Soldani,<sup>e,f</sup> A. Triossi,<sup>o</sup> E. Vallazza,<sup>f</sup> S. Ventura,<sup>h</sup> M. Zanetti.<sup>n,h</sup>

<sup>a</sup>Università degli Studi di Torino - Torino, Italy

<sup>b</sup>INFN Sezione di Torino - Torino, Italy

<sup>c</sup>INFN Laboratori Nazionali di Frascati - Frascati, Italy

<sup>d</sup>INFN Sezione di Roma - Rome, Italy

<sup>e</sup>Università degli Studi dell'Insubria - Como, Italy

<sup>f</sup>INFN Sezione di Milano Bicocca - Milan, Italy

<sup>g</sup>INFN Sezione di Ferrara - Ferrara, Italy

<sup>h</sup>INFN Sezione di Padova - Padova, Italy

<sup>i</sup>INFN Sezione di Trieste - Trieste, Italy

<sup>l</sup>Università di Roma La Sapienza - Rome, Italy

<sup>m</sup>CERN - Geneva, Switzerland

<sup>n</sup>Università di Padova - Padova, Italy

<sup>o</sup>Institut Pluridisciplinaire Hubert Curien, Strasbourg, France

E-mail: [bertolin@pd.infn.it](mailto:bertolin@pd.infn.it)

**ABSTRACT:** This paper presents the double arm dipole spectrometer experimental setup developed in the framework of the Low Emittance Muon Accelerator (LEMMA) project. This project aims at proving the production of small emittance muons from positron annihilation on electrons at rest. The availability of an intense source of cooled muon beams is one of the main challenges that have to be met before the attractive idea of a muon collider can be turned into a realistic project. The presented setup has been implemented in a test beam campaign performed at CERN in Summer 2018. The results achieved are presented and compared with the corresponding simulations.

**KEYWORDS:** Muon collider, low emittance muon beam.

---

## Contents

<b>1</b>	<b>Introduction</b>	<b>1</b>
<b>2</b>	<b>Experimental setup</b>	<b>2</b>
<b>3</b>	<b>Simulations</b>	<b>4</b>
3.1	Analytical computations	4
3.2	Monte Carlo simulations	4
<b>4</b>	<b>Data taking and analysis strategy</b>	<b>4</b>
<b>5</b>	<b>Results</b>	<b>6</b>
5.1	Data to MC comparisons	6
5.2	Raw emittance	8
5.3	$x$ and $x'$ distributions	10
<b>6</b>	<b>Conclusions</b>	<b>10</b>

---

## 1 Introduction

In order to further consolidate the present knowledge of the Standard Model and to look for deviations from its predictions that would signal new physics effects, a new generation of hadron–hadron or electron–positron colliders is being put forward. However, also the idea of a muon collider is attractive because such a machine would provide the high centre of mass energy typical of a hadron–hadron machine by colliding fundamental particles as in an electron–positron machine. Hence a muon collider can explore the multi–TeV energy frontier as well as be used as a Higgs factory. However a muon collider has to face quite a few challenges mainly due to the fact that muons decay with a lifetime of  $2.2 \mu\text{sec}$  at rest. The production of low emittance muon/antimuon beams to be fed into the accelerator complex is one of the main challenges.

The LEMMA project [1] is studying the possibility of a muon collider where muons are produced from the  $e^+e^-$  annihilation process. In the current scheme a high intensity positron beam, above the production energy threshold at 43.7 GeV, collides with a fixed target. In this way, muons are produced with a small divergence and energy spread, resulting in a small emittance that could avoid the need of beam cooling. Moreover, muons life time is extended to about 0.4 ms because of the asymmetrical collisions. On the other hand, the small cross section of the  $e^+e^- \rightarrow \mu^+\mu^-$  process ( $< 1 \mu\text{barn}$ ) requires a high positron rate on the target to produce enough muons in less than one muon life time, forcing the target to operate in a high power deposition regime. The positron rate could be reduced recirculating the positron beam many times through the target. The alternative strategy of getting muons from tertiary production by protons requires the development of a new muon cooling technique that is pursued by the MICE [2, 3] project.

The initial LEMMA muon production scheme, presented in [4–7], uses a train of 100 bunches with a charge of  $10^{12}$  positrons each, where bunches are separated by 200 ns. The train is recirculated 100 times over a 6 km ring and intercepted by the fixed target. The produced muon pairs are then collected in two separated 60 m long accumulator rings overlapping the positron ring at the target location in a way such as to produce new mouns while at the same time storing the old ones with minimal emittance growth. Other alternative schemes are now being considered [8, 9] to mitigate the average power deposition in the target and the demands on the positron source.

Regardless of the variations of the muon production scheme, the keystone of the project is the target. It sets the muon production efficiency, i.e. the number of muon pairs produced per incoming positron ( $\mu/e^+$ ), and the limit on the minimum emittance because of beam divergence, multiple scattering and energy loss from bremsstrahlung. The balance between beam dynamics and thermo-mechanical considerations pointed out to the use of thin low-Z solid materials. Beryllium has been the preferred material to study, but others have been also considered. In particular, a 3 mm thick solid Be target, which corresponds to less than 1% of a radiation length,  $X_0$ , has been used to give estimations on the minimum emittance because of its short length (i.e. no contribution to emittance from the beam divergence inside the target nor multiple scattering). For such a thin target, simulations in Geant4 [10] and Accelerator Toolbox [11] have been performed to study the beams phase space [12]. Increasing the length of the target clearly goes in the direction of enhancing the number of muons but the effects of muon beam divergence and multiple scattering inside the target are no longer negligible and require further study.

The following sections describe first the double arm dipole spectrometer experimental setup developed to perform measurements sensitive to the emittance of the final state muons produced by the annihilation process  $e^+e^- \rightarrow \mu^+\mu^-$ . This setup has been implemented in a test beam campaign performed at CERN in Summer 2018. Analytical computations as well as detailed Monte Carlo simulations have been developed to get predictions that could be compared to the data. The data taking and analysis strategy are discussed first, reached results are presented and compared to the corresponding simulations. Conclusions are given in the last section.

## 2 Experimental setup

The experimental setup was designed to measure with high precision trajectories and momenta of the two final state muons as well as the direction of interacting positrons. The layout of the setup is schematically shown in Fig. 1, with the right-handed coordinate system defined by the  $z$ -axis pointing along the direction of the positron beam, the  $y$ -axis pointing to the roof of the experimental hall and the  $x$ -axis orthogonal to the other two axes. The total length of the apparatus in the  $z$  direction was about 23 m.

Initially the positron beam passed through a fast-response plastic scintillator and a pair of silicon microstrip sensors before hitting the target. The silicon sensors allowed a measurement of the direction and position of the positron beam on the target, while the scintillator was used for trigger purposes. In this experiment all the silicon sensors were formed by two layers of microstrips with orthogonal directions, and allowed a measurement of the hit positions and the corresponding pulse height in the  $x$   $y$  plane. The silicon sensors upstream of the target were  $2 \times 2$  cm<sup>2</sup> in size and provided position measurements with a microstrip pitch of 50  $\mu$ m [13]. In the following the

$z$ -position of the first silicon detector was considered as the origin of the  $z$ -axis ( $z = 0$ ). The measured detectors and target  $z$ -positions of the August 2018 setup are given in the following. They are compatible within a few centimeters with the September 2018 setup. The second silicon sensor was placed in  $z = 359$  cm, while the center of the target was located in  $z = 458$  cm.

Muon pairs produced in the target material passed through a vacuum beam pipe and another pair of silicon sensors, one before ( $z = 467$  cm) and one after the pipe ( $z = 1410$  cm), which measured the direction of the muons before passing through the 2 T magnetic field created by a dipole magnet. The two silicon microstrip sensors downstream of the target and upstream of the magnet were  $9.5 \times 9.5$  cm<sup>2</sup> in size and had a pitch of 242  $\mu$ m [14]. The center of the dipole magnet was at  $z = 1591$  cm and the field extended in a region of approximately  $\pm 1000$  cm.

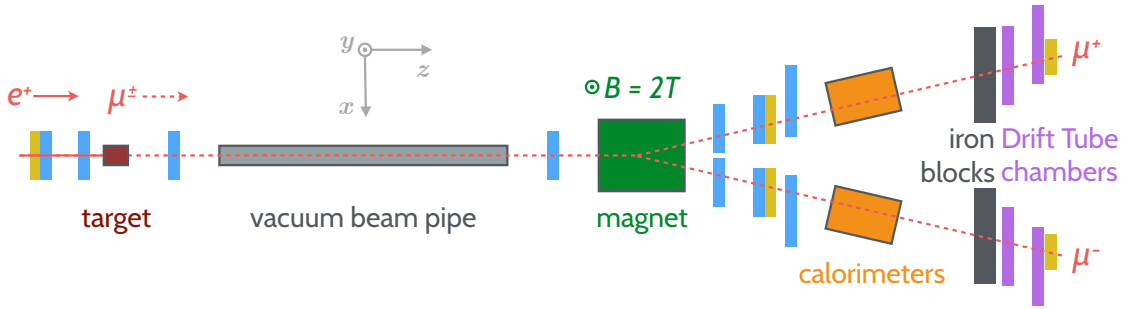


**Figure 1.** Schematic view of the test beam experimental setup as used in the testbeam of August-September 2018. The  $xz$  plane view is shown, with  $x$  and  $z$  axes defined in the text. All the components of the setup are marked in the figure except for a sequence of silicon tracking sensors (in blue) and plastic scintillators (in yellow) that were used to trigger the data acquisition.

Downstream of the magnet the paths of the muons diverged in two arms. Momenta were measured using measurements upstream and downstream of the bending magnet. In each arm a muon passed through three layers of silicon microstrip sensors ( $z = 1791$  cm,  $z = 1913$  cm and  $z = 2042$  cm) followed by a calorimeter and by two layers of drift tube (DT) muon chambers (first layer at  $z = 2311$  cm). The two silicon sensors upstream and closer to the magnet were  $8 \times 8$  cm<sup>2</sup> in size and had a pitch of 228  $\mu$ m, while the silicon sensor in front of the DT chamber was  $18 \times 18$  cm<sup>2</sup> with a pitch of 456  $\mu$ m [14].

The DT chambers employed the same technology used by the CMS experiment at LHC [15]. The DT chambers consisted of four layers of wires each, providing up to 8 hits in the  $xz$  plane in each arm. The expected spatial resolution along the  $x$ -axis was about 150  $\mu$ m.

Positrons were expected to deposit most of their energy in the calorimeter. Additional leakage was absorbed by the iron shielding placed downstream so that only  $\mu^\pm$  tracks were expected to reach the DT chambers. Each calorimeter consisted of a lead-glass ( $\text{PbWO}_4$ ) section followed by a Cherenkov section, to differentiate between electron and muon tracks.

Finally a plastic scintillator was positioned behind the last DT chamber in each arm. Three plastic scintillators, one at entry point and two at the end of each arm, served as trigger for the shared silicon sensors and calorimeters data acquisition system (DAQ) requiring a coincidence between all of them. The DT chambers were using an independent trigger-less DAQ system with with an

acquisition rate of 40 MHz. The trigger signal from the scintillators was shared between the two DAQ systems for offline synchronisation and event building.

### 3 Simulations

#### 3.1 Analytical computations

Analytical computations have been performed to get predictions for the emittance value of the muons produced by the process  $e^+e^- \rightarrow \mu^+\mu^-$  in a plane perpendicular to the  $z$ -axis at the  $z$ -coordinate corresponding to the target end position. The ad-hoc developed EEMUMU code generates the muons by taking into account the incoming positron beam features (spatial and angular distributions of the positrons at the entrance of the target) and the target material. The code has been benchmarked against Babayaga [16] and Whizard [17] in case of an ideal zero emittance positron beam impinging on an empty target. To match as accurately as possible the experimental conditions a positron beam characterized by a flat distribution in a square of  $2 \times 2 \text{ cm}^2$ , to match the shape of the silicon detectors upstream of the target, a gaussian distributed angular spread of  $335 \mu\text{rad}$ , with a cutoff at  $\pm 450 \mu\text{rad}$ , and an energy of 45 GeV, impinging on a cylindrical beryllium target 6 cm long was simulated. This resulted in an expected geometrical emittance of  $3221 \text{ nm} \times \text{rad}$ . Clearly this analytical computation can not take into account track reconstruction effects but this result is a useful cross check for the corresponding values found from both the detailed Monte Carlo simulations and the data.

#### 3.2 Monte Carlo simulations

The whole experimental setup has been implemented in the Geant4 simulation toolkit [10]. All relevant volumes, silicon detectors, calorimeters, muon chambers and iron shieldings, have been simulated with their exact shape and material composition in order to correctly model the energy release and particles attenuation. As far as primary particles are concerned, several options have been implemented: besides the possibility to simulate a 45 GeV positron beam along the  $z$ -axis, with characteristics similar to the experimental one, also the possibility to use a  $\mu^+\mu^-$  pairs input file in the HEPMC format has been implemented. This allowed the simulation of a sufficient amount of  $e^+e^- \rightarrow \mu^+\mu^-$  events within a reasonable time, given the very low cross section of the annihilation process. Similarly, also the possibility to simulate Bhabha events via external input files has been implemented. The magnetic field could be simulated in two ways: either with a constant dipole value inside the magnet footprint or with the analytical field map provided for the specific magnet used in the experiment. This map is depending also on the operating current. The output of the simulation is given by *.root* files in which on a primary-by-primary particle basis each interaction in any of the volumes is recorded.

### 4 Data taking and analysis strategy

Two test beam data-taking campaigns have been conducted in August 2018 and September 2018, for approximately one week each time. At the beginning of each period, calibration runs have been recorded in different configurations. In particular  $\mu^+$  beams at energies of 22 GeV without target and with both magnetic field directions have been used for alignment of silicon detectors and DT

muon chambers in both arms. In August 2018 physics runs were recorded with a 45 GeV positron beam impinging on a beryllium cylindrical target. The beryllium target was 60 mm length and with a 40 mm diameter. In September 2018 physics runs were recorded with positron beams of several energies (45, 46.5 and 49 GeV) impinging on the same beryllium target, and runs with a 45 GeV positron beam on carbon cylindrical targets with different length (60 mm and 20 mm) and same diameter (40 mm). The "nominal" positron beam had a pulsed shape with an intensity of  $\sim 5 \times 10^6$  positrons per spill.

The goal of the data analysis is to identify  $e^+e^- \rightarrow \mu^+\mu^-$  events, measure the muon trajectories in the  $xz$  plane, measure the muon momenta and determine the interacting positron direction. The main background process was the Bhabha scattering  $e^+e^- \rightarrow e^+e^-$ . Most of the electrons did not have enough energy to pass through the calorimeters, therefore events with two muons, one for each arm, were identified by requiring one track per DT muon chamber. DT tracks were used as seeds for the pattern recognition. Hits were added starting from the DT chambers and moving backwards to the other detectors with the following procedure:

1. for each arm, hits in the silicon detectors downstream to the magnet were selected if they formed, in the  $xz$  plane, a straight line with the corresponding DT track; fits to these hits were performed to obtain one downstream muon track per arm;
2. a preliminary estimation of  $\mu^+$  and  $\mu^-$  momenta was obtained using the angles formed by downstream tracks and  $z$ -axis;
3.  $\mu^+$  and  $\mu^-$   $x$ -positions in the silicon detector before the magnet were extrapolated propagating the downstream tracks through the magnetic field, according to their estimated momenta; the two hits in this detector nearest to the extrapolated  $\mu^+$  and  $\mu^-$  positions were added to the tracks;
4. a global fit that involved all the already-selected hits was performed to add the best  $\mu^+$  and  $\mu^-$  hits in the first silicon detector after the target. Spline functions (straight line-parabola-straight line) were used to describe the muon trajectories in the  $xz$  plane at this stage;
5. selected  $\mu^+$  and  $\mu^-$  tracks were then re-fitted to obtain the  $xz$  trajectories and the measured momenta. A cut on the goodness of fit was applied to remove the combinatorial background.

The muon reconstruction algorithm was validated in the calibration Runs, where muons were reconstructed and their measured momenta were compared with the nominal known value. Calibration runs were also used to verify that the electron mis-identification in the DT muon chambers was negligible.

The interacting positron direction was assumed to form a vertex with the  $\mu^+$  and  $\mu^-$  trajectories in the target region. Therefore it was obtained by considering the combinations of hits in the first two silicon detectors, and performing a vertex fit together with the  $\mu^+\mu^-$  tracks. The positron direction was obtained from the hits pair that gives the best goodness of fit. Hence this procedure allowed to properly handle the events in which more than one positron was reconstructed from the data of the first two silicon detectors. The observed positron multiplicity, as obtained from a representative data sample with looser cuts, is shown in Fig. 2.

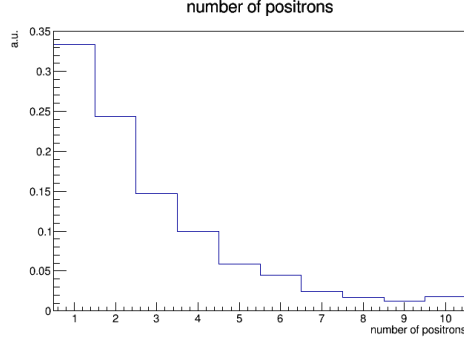


**Figure 2.** Distribution of the number of reconstructed positrons using the hits in the first two silicon detectors.

## 5 Results

### 5.1 Data to MC comparisons

In order to test the reconstruction algorithms presented in the previous section several kinematic quantities, as obtained from the final August 2018 data sample, are compared with the Geant4 simulation expectations. The final data sample is formed by events with two well reconstructed muon tracks, each with a measured momentum, and an incoming positron. The position and direction of the positron were measured by the silicon planes upstream of the target. Moreover these three tracks should match to a common vertex, the positron annihilation point in the target. A sample of 61 events fulfilling the above conditions was obtained.

The first kinematic quantity considered is the reconstructed angle in the bending plane at track start. The corresponding data and simulation shapes are compared in Fig. 3 separately for positive, left plot, and negative, right plot, reconstructed muon tracks. The reconstructed distributions show well collimated tracks, as expected from the Geant4 simulation.

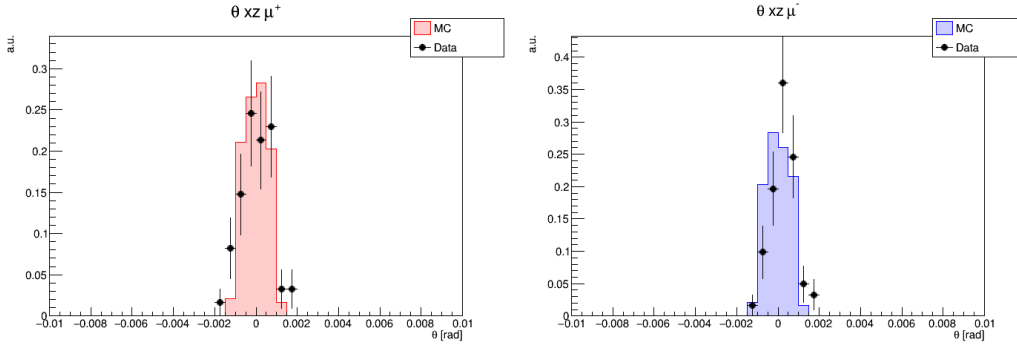


**Figure 3.** Reconstructed angle in the bending plane at track start for positively (left) and negatively (right) charged tracks, in events where both are reaching the muon detectors. Data are shown by the dots, simulations by the filled histograms. Both data and simulations are normalized to unit area.

A similar comparison is performed for the reconstructed tracks momenta in Fig. 4. As expected

from the simulation, the reconstructed distributions are almost flat in the range between 18 and 26 GeV.

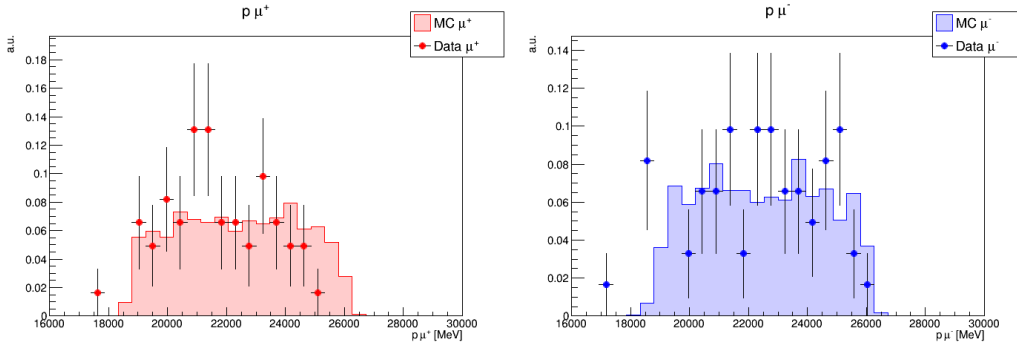


**Figure 4.** Reconstructed momentum for positively (left) and negatively (right) charged tracks, in events where both are reaching the muon detectors. Data are shown by the dots, simulations by the filled histograms. Both data and simulations are normalized to unit area.

As a trivial consequence of energy conservation in the process  $e^+e^- \rightarrow \mu^+\mu^-$  on a target at rest, the sum of the muons momenta should peak at the fixed energy of the incoming positron beam. The observed experimental spread depends mostly on the muon track momentum resolution convoluted with the energy spread of the incoming positron beam. The measured shape is shown in Fig. 5 and compared to a simulation obtained by smearing the generated muon track momenta by 3%. This resolution is consistent with what obtained from single muon calibration runs with fixed momentum in the range 18 and 26 GeV. A few data points occur at values about 10% smaller than the main peak, around 40 GeV. A similar behaviour is also seen when analyzing single muon calibration runs. Hence events around 40 GeV are more likely to be due to non Gaussian tails in the momentum reconstruction rather than being an unwanted background contribution.

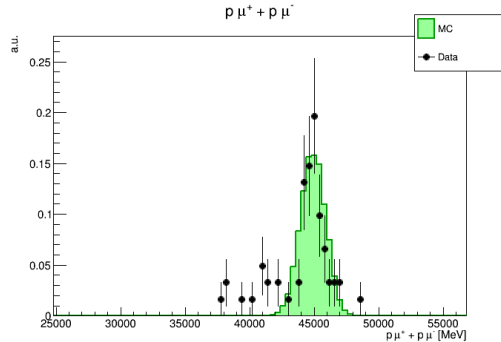


**Figure 5.** Reconstructed sum of the muon track momenta. Data are shown by the dots. The filled histogram corresponds to the result of a simulation assuming a 3% energy resolution on the track momenta. Both data and simulation are normalized to unit area.

The last kinematic quantity considered is the invariant mass of the two muon tracks, Fig. 6. As the reaction  $e^+e^- \rightarrow \mu^+\mu^-$  is measured at the threshold energy the naive expectation is a peak



at twice the muon mass, i.e. about 212 MeV. This naive expectation, well visible in the selected events, is also confirmed by the simulation results.

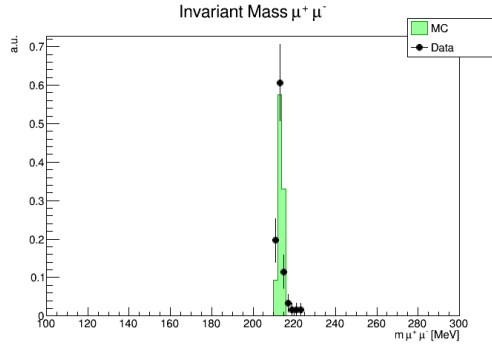


**Figure 6.** Invariant mass of the muon track pairs. Data are shown by the dots. The filled histogram corresponds to the result of the simulation. Both data and simulation are normalized to unit area.

Two main sources of inefficiency contribute to the modest final number of collected events in the August 2018 data taking period, namely:

- the rate limitation of the silicon detectors and calorimeters readout system available, at about 500 Hz, was introducing a large dead time given the observed trigger rate;
- the lack of redundancy in the measurements performed in the region between the target and the magnet. In order to have well measured tracks, hits in both of the two available detectors had to be requested for both muon tracks. This stringent condition leads to an additional reduction of the efficiency.

In September 2018 to cure the too large dead time of the August runs an additional scintillator was added to trigger on events with a track in each arm crossing the corresponding muon chamber, see Fig. 1. This action partially cured the dead time issue, but due to a hardware misconfiguration the trigger efficiency was very low. Using the trigger-less data recorded by the DT system, the efficiency could be estimated to be as low as  $\sim 2\%$ . Once the hardware issue was fixed the estimated efficiency went up to  $\sim 10\%$ . A similar estimate of the efficiency was obtained for the August 2018 runs.

A set of data corresponding to a 45 GeV positron beam impinging on a 2 cm thick carbon target recorded after the hardware misconfiguration fix was analysed. Applying all the analysis cuts except the positron–muon pair vertex matching a sample of 157 events was obtained. These reduced to 9 when the positron–muon pair matching condition was applied. Additional investigations showed that the "geometrical overlap" of the silicon detectors used in coincidence to tag the incoming positrons was significantly worse in September 2018 w.r.t August. This resulted in a severely limited efficiency for matching the recorded muon pair with the positron that originated it.

## 5.2 Raw emittance

The raw emittance is defined in the  $x(\mu) x'(\mu)$  plane where  $x(\mu)$  is the extrapolated position along the  $x$ -axis of the track at a reference plane taken to be perpendicular to the  $z$ -axis and at a  $z$  position

corresponding to the target end point.  $x'(\mu)$  is the corresponding extrapolated local track slope. The observed distributions in the  $x(\mu)$   $x'(\mu)$  plane, as obtained from the August 2018 data sample, are shown separately for positive and negative muons in Fig. 7. No efficiency corrections are applied. The emittance is computed using an unbinned algorithm not requiring the distribution to be centered at the origin of the  $x(\mu)$   $x'(\mu)$  plane [18]. The numerical values obtained are:

$$\begin{aligned}\epsilon(\mu^+) &= (3.53 \pm 0.38 \text{ (stat.)}) \cdot 10^3 \text{ nm} \times \text{rad} \\ \epsilon(\mu^-) &= (2.89 \pm 0.29 \text{ (stat.)}) \cdot 10^3 \text{ nm} \times \text{rad}\end{aligned}$$

where the uncertainty has been obtained from the bootstrap method applied to the 61 events data sample. The following main sources of systematic uncertainties have been considered and evaluated using simulated events or positron calibration runs:

- variations of the spatial resolution of the tracking detectors;
- uncertainty on  $e^+e^- \rightarrow e^+e^-$  background contamination.

Only the contribution from the first source has an impact at the percent level. Hence systematic uncertainties are much smaller with respect to the statistical error and neglected.

Corresponding predictions have been obtained from the MC simulation. Events were generated using an incoming positron beam with the same kinematic properties, in terms of spatial distribution and divergence, as measured in the data with the two silicon detectors upstream of the target. These have been reported in Sec. 3.1. Varying the boundaries of the flat spatial distribution or the divergence leads to uncertainties in the predicted raw emittance of about 5 %. Averaging the  $\mu^+$  and  $\mu^-$  simulation results leads to a predicted value of:

$$(2.76 \pm 0.15 \text{ (modeling)}) \cdot 10^3 \text{ nm} \times \text{rad},$$

in fair agreement with the experimentally measured values.

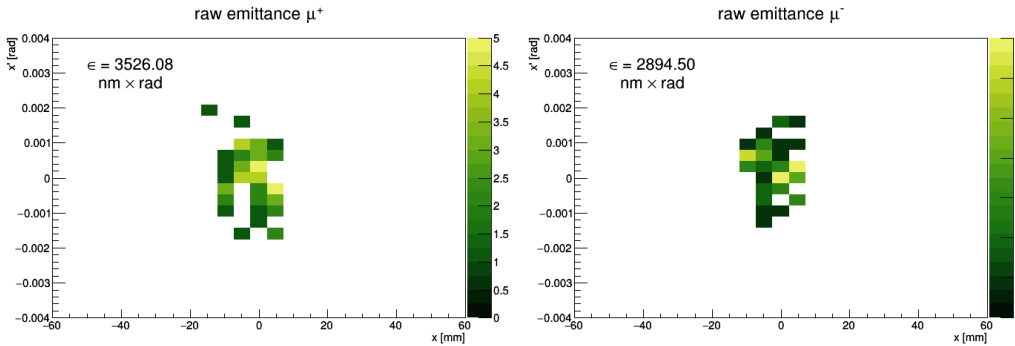


**Figure 7.** Raw emittance of the positive (left) and negative (right) tracks. The numerical result is shown as an insert in the plot.

### 5.3 $x$ and $x'$ distributions

The measured raw emittance values are so large because a very broad distribution in  $x$  and  $y$  was chosen for the incoming positron beam. This choice was driven in order to minimize the chance of having two nearby positrons and assigning the wrong one to the measured  $\mu^+\mu^-$  pair. This resulted in an almost uniform positron distribution in the  $x$  range between  $-10$  mm and  $+10$  mm. This almost uniform  $x(\mu)$  distribution is still visible in Fig. 3, at the reference plane  $z$  position. Hence the  $x(\mu)$  and  $x'(\mu)$  values that corresponds to the raw emittance have to be corrected by:

$$\begin{aligned} x &= x(\mu) - x(e^+) \\ x' &= x'(\mu) - x'(e^+) \end{aligned}$$

where  $x(e^+)$  and  $x'(e^+)$  are the positions and local slopes obtained from the geometrical extrapolation of the incoming positron to the reference plane.

Simulation studies using generated Geant4 quantities show a width of the  $x$  distribution around  $30 \mu\text{m}$ . At the reconstruction level the observed width that can be achieved with the available experimental setup is significantly larger, around  $100 \mu\text{m}$ . Hence no useful measurement of the  $x$  distribution can be performed.

A better accuracy is reached on the  $x'(\mu)$  and  $x'(e^+)$  measurements. The  $x'$  distribution measured in data is shown in Fig. 8 together with the corresponding simulation result. A fair agreement is found. The drop around  $x' = 0$ , well visible both in data and simulations, is due to the fact that a fraction of the events that have small values of  $x'$  for both muon tracks. A small  $x'$  value corresponds to a small slope. Hence these tracks, produced at the same vertex, will travel almost parallel up to the magnetic field region. Due to this track overlap the track reconstruction efficiency is lower for this particular class of events. The determination of a reliable efficiency correction to account for this effect is not possible given the very limited data sample available to validate it.

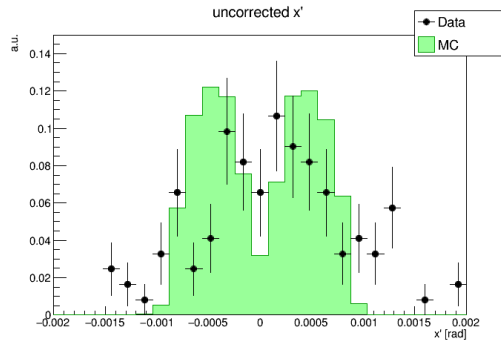


**Figure 8.**  $x'$  distribution: data are shown by the dots, the continuous histogram corresponds to the result of the simulation. Both data and simulation are normalized to unit area.

## 6 Conclusions

The  $e^+e^- \rightarrow \mu^+\mu^-$  annihilation process at threshold energy has been studied with particular emphasis on the kinematic properties of the final state muons. Several unexpected difficulties

during the acquisition campaigns lead to a yield of 61 events. However for these events both the incoming positron and the outgoing muons are well measured and correlated. So these can be used to get a first estimate of the raw emittance that, within the large data statistical uncertainty, is consistent with analytical calculations and more detailed simulations of the full detector setup. These data also allowed a comparison of the observed uncorrected  $x'$  distribution to simulations. A fair agreement is found. In order to subtract the large emittance of the incoming positron beam from the measured raw muon emittance i.e. to provide a measurement of the achievable muon beam emittance independent from the incoming positron beam characteristics, more accurate tracking devices, alignment infrastructures and more efficient trigger and readout systems will be needed. Such a setup could then be used for future studies and optimizations of the LEMMA muon production scheme.

## Acknowledgements

We would like to warmly thanks the SPS staff and the Large Scale Metrology group, in particular Henrik Wilkens and Nikolaos Charitonidis, for their support during installation and data taking. This work has been partially supported by the ERC CoG GA 615089 CRYSBEM.

## References

- [1] M. Antonelli, M. Boscolo, R. Di Nardo and P. Raimondi, *Novel proposal for a low emittance muon beam using positron beam on target*, Nucl. Instrum. Meth. A **807** (2016) 101.
- [2] T. A. Mohayai *et al.*, *First Demonstration of Ionization Cooling in MICE*, Proc. 9th Int. Particle Accelerator Conf. (IPAC'18) (2018) 4.
- [3] M. Bogomilov *et al.*, *First demonstration of ionization cooling by the Muon Ionization Cooling Experiment*, arXiv:1907.08562.
- [4] M. Antonelli *et al.*, *Very Low Emittance Muon Beam using Positron Beam on Target*, Proc. of the 7th Int. Particle Accelerator Conf. (IPAC'16) (2016) 1536.
- [5] M. Boscolo *et al.*, *Studies of a Scheme for Low Emittance Muon Beam Production From Positrons on Target*, Proc. 8th Int. Particle Accelerator Conf. (IPAC'17) (2017) 2486.
- [6] M. Boscolo *et al.*, *Low emittance muon accelerator studies with production from positrons on target*, Phys. Rev. Accel. Beams **21** (2018) 061005.
- [7] D. Alesini *et al.*, *Positron driven muon source for a muon collider*, arXiv:1905.05747.
- [8] M. E. Biagini *et al.*, *Positron Driven Muon Source for a Muon Collider: Recent Developments*, Proc. 10th Int. Particle Accelerator Conf. (IPAC'19) (2019) 49.
- [9] O. R. Blanco-García *et al.*, *Multi-Target Lattice for Muon Production From  $e^+$  Beam Annihilation on Target*, Proc. 10th Int. Particle Accelerator Conf. (IPAC'19) (2019) 578.
- [10] S. Agostinelli, *et al.*, *GEANT4: A Simulation toolkit*, Nucl. Instrum. Meth. A **506** (2003) 250.
- [11] B. Nash *et al.*, *New Functionality for Beam Dynamics in Accelerator Toolbox (AT)*, Proc. 6th Int. Particle Accelerator Conf. (IPAC'15) (2015) 113.
- [12] M. Boscolo *et al.*, *Muon Accumulator Ring Requirements for a Low Emittance Muon Collider from Positrons on Target*, Proc. 9th Int. Particle Accelerator Conf. (IPAC'18) (2018) 330.

- [13] D. Lietti *et al.*, *A microstrip silicon telescope for high performance particle tracking*, Nucl. Instr. Meth. A **729** (2013) 527.
- [14] G. Barbiellini *et al.*, *The AGILE silicon tracker: testbeam results of the prototype silicon detector*, Nucl. Instr. Meth. A **490** (2002) 146.
- [15] S. Chatrchyan *et al.*, *The CMS experiment at the CERN LHC*, J. Instrum. 3 (2008) S08004.
- [16] C. M. Carloni Calame, G. Montagna, O. Nicosini and F. Piccinini, *The BABAYAGA event generator*, Nucl. Phys. Proc. Suppl. **131** (2004) 48.
- [17] W. Kilian, T. Ohl and J. Reuter, *WHIZARD: Simulating Multi-Particle Processes at LHC and ILC*, Eur. Phys. J. C **71** (2011) 1742.
- [18] K. Floettmann, *Some basic features of the beam emittance*, Phys. Rev. Special Topics - Accelerators and Beams 6 (2003) 034202.